OPEN ACCESS Freely available online

PLoS one

Effects of Anti-VEGF on Predicted Antibody Biodistribution: Roles of Vascular Volume, Interstitial Volume, and Blood Flow

C. Andrew Boswell[1]*, Gregory Z. Ferl[1], Eduardo E. Mundo[1], Daniela Bumbaca[1], Michelle G. Schweiger[2], Frank-Peter Theil[1], Paul J. Fielder[1], Leslie A. Khawli[1]

1 Department of Pharmacokinetic and Pharmacodynamic Sciences, Genentech Inc., South San Francisco, California, United States of America, **2** Department of Investigative Safety Assessment, Genentech Inc., South San Francisco, California, United States of America

Abstract

Background: The identification of clinically meaningful and predictive models of disposition kinetics for cancer therapeutics is an ongoing pursuit in drug development. In particular, the growing interest in preclinical evaluation of anti-angiogenic agents alone or in combination with other drugs requires a complete understanding of the associated physiological consequences.

Methodology/Principal Findings: Technescan™ PYP™, a clinically utilized radiopharmaceutical, was used to measure tissue vascular volumes in beige nude mice that were naïve or administered a single intravenous bolus dose of a murine anti-vascular endothelial growth factor (anti-VEGF) antibody (10 mg/kg) 24 h prior to assay. Anti-VEGF had no significant effect ($p>0.05$) on the fractional vascular volumes of any tissues studied; these findings were further supported by single photon emission computed tomographic imaging. In addition, apart from a borderline significant increase ($p = 0.048$) in mean hepatic blood flow, no significant anti-VEGF-induced differences were observed ($p>0.05$) in two additional physiological parameters, interstitial fluid volume and the organ blood flow rate, measured using indium-111-pentetate and rubidium-86 chloride, respectively. Areas under the concentration-time curves generated by a physiologically-based pharmacokinetic model changed substantially (>25%) in several tissues when model parameters describing compartmental volumes and blood flow rates were switched from literature to our experimentally derived values. However, negligible changes in predicted tissue exposure were observed when comparing simulations based on parameters measured in naïve versus anti-VEGF-administered mice.

Conclusions/Significance: These observations may foster an enhanced understanding of anti-VEGF effects in murine tissues and, in particular, may be useful in modeling antibody uptake alone or in combination with anti-VEGF.

Citation: Boswell CA, Ferl GZ, Mundo EE, Bumbaca D, Schweiger MG, et al. (2011) Effects of Anti-VEGF on Predicted Antibody Biodistribution: Roles of Vascular Volume, Interstitial Volume, and Blood Flow. PLoS ONE 6(3): e17874. doi:10.1371/journal.pone.0017874

Editor: Juri Gelovani, University of Texas, M.D. Anderson Cancer Center, United States of America

Received December 23, 2010; **Accepted** February 11, 2011; **Published** March 15, 2011

Funding: The authors have no support or funding to report.

Competing Interests: The authors have read the journal's policy and have the following conflicts: All authors are paid employees of Genentech, a member of the Roche Group, and hold financial interest in Roche in the form of stocks and/or options. Two drugs mentioned in this manuscript, trastuzumab and bevacizumab, are marketed by Genentech/Roche. In addition, CAB serves as an Academic Editor for PLoS ONE. None of these financial or competing interests alters the authors' adherence to all PLoS ONE policies on sharing data and materials.

* E-mail: boswell.andy@gene.com

Introduction

The absence of many physiological processes *in vitro* and interspecies differences *in vivo* can confound direct comparisons of *in vitro*, preclinical, and clinical data [1,2]. A vast array of physiological data for humans and laboratory species is available in the literature [3,4,5,6]; however, it should be utilized with an understanding of its limitations. Significant physiological variability across species, age, breed, disease status, drug treatment, and time of day [7] motivates direct measurement of relevant physiological properties or processes whenever possible [8].

The measurable effects of anti-vascular endothelial growth factor (anti-VEGF) therapy on tumors in preclinical and clinical settings include reductions in vascular density, vascular volume, vessel permeability, and/or blood flow [9]; however, changes have also been reported for small molecule VEGF inhibitors in non-malignant tissues [10]. For instance, inhibition of VEGF in mice using non-antibody-based anti-angiogenic agents induced distinct physiological changes, including reduced cardiac output, changes in blood glucose regulation, reduction of endothelial cell fenestrations, and significant capillary regression in several tissues [10]. Several VEGF inhibitors have yielded measureable, although generally manageable, adverse effects in the clinical oncology setting [11], thus encouraging further studies into the underlying mechanisms behind the observed biological changes.

Preclinical studies evaluating the effects of anti-angiogenic antibodies on all aspects of tissue physiology may have important implications, especially given the increased clinical interest in antibodies against angiogenic targets [9]. The present study investigates the impact of a cross-species anti-VEGF antibody

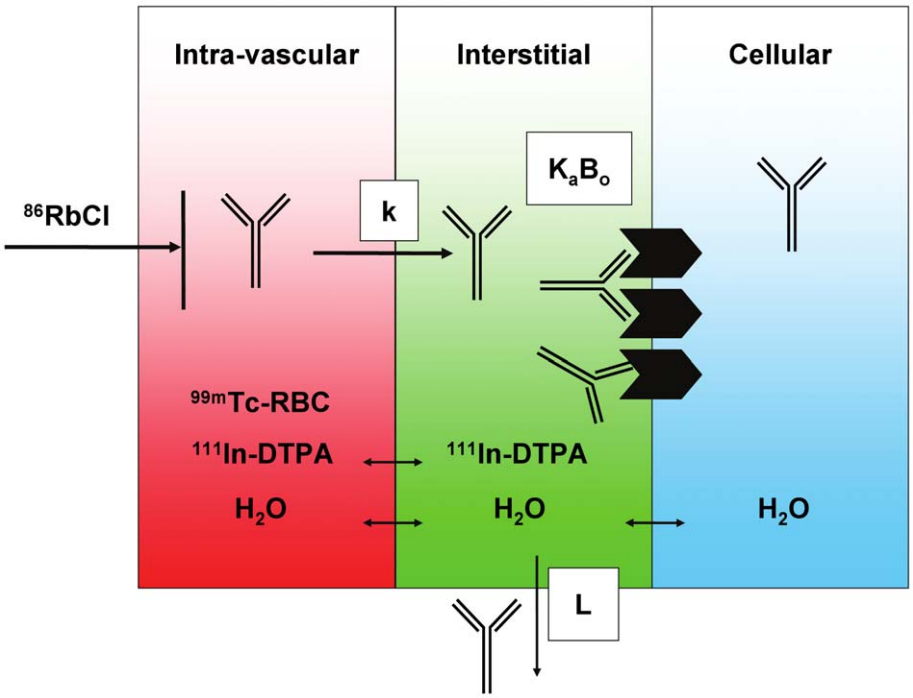

Figure 1. Conceptual illustration of techniques used to measure physiological parameters relevant to antibody uptake in tissues. The tissue is divided into vascular, interstitial, and cellular compartments (depicted in red, green, and blue, respectively). The blood space (V_v) may be measured using ^{99m}Tc-labeled red blood cells (RBC), while the extracellular (i.e. V_v+V_i) space is measured by infusion of ^{111}In-DTPA. The rate of blood flow (Q) to the tissue may be measured as the proportion of a bolus dose of ^{86}RbCl that enters the tissue in a brief time interval. The antibody's receptor, if present, may be expressed on the cell surface, exposed to the interstitial fluid. An antibody in circulation may extravasate from blood into interstitial space at a rate (k), where it may encounter a number (B_o) of receptors for which it has binding affinity (K_a). The antibody may also return to circulation via lymphatic flow (L).
doi:10.1371/journal.pone.0017874.g001

[12], B20-4.1, on the vascular volumes (V_v), interstitial fluid volumes (V_i), and regional rates of blood flow (Q) for selected tissues in nude mice (**Figure 1**).

Physiologically-based pharmacokinetic (PBPK) modeling can aid in understanding mechanisms of tissue uptake and can predict, by means of inter-species scaling, tissue concentrations of therapeutic antibodies in humans based on preclinical PK data of molecules currently in development [13]. The success of PBPK modeling, however, is dependent on parameter values that accurately reflect *in vivo* tissue physiological conditions. Importantly, a sensitivity analysis of a previously reported PBPK model implicated V_v and V_i as two of the most influential parameters on antibody concentration in tissues, particularly at early time points [5]. In addition, preclinical and clinical magnetic resonance imaging studies have demonstrated changes in parameters describing V_v and Q and/or vessel permeability in tumors following anti-VEGF treatment [9]. In this context, tissue uptake of a generic IgG was predicted by physiologically-based pharmacokinetic (PBPK) modeling (**Figure 2**) using V_v, V_i and Q values obtained from the literature, measured in naïve mice, or measured in mice receiving anti-VEGF; predicted uptake values were compared to experimental uptake data for a model antibody (trastuzumab) in nude mice.

Results

Vascular volume

Successful RBC labeling with ^{99m}Tc was evident due to observed association of the vast majority of radioactivity with the RBC pellet fraction for both naïve and B20-4.1-administered mice (**Figure 3**). For the direct RBC labeling method, the mean %ID/g values for the naïve and B20-4.1-administered mice, respectively, were 0.79±0.14 vs. 0.75±0.11 in plasma, 39.6±14.2 vs. 49.7±4.4 in whole blood, and 77.1±27.3 vs. 97.3±9.3 in the RBC pellet. To ensure that the anti-angiogenic effects did not interfere with the measurement, a refined indirect method for measuring V_v [2] allowed red blood cell (RBC) labeling to be performed in a separate cohort of naïve (i.e. receiving no anti-VEGF) mice. For the indirect method, the mean %ID/g values for the naïve and B20-4.1-administered mice, respectively, were 0.63±0.19 vs. 0.57±0.13 in plasma, 55.1±2.5 vs. 53.3±3.6 in whole blood, and 98.3±6.2 vs. 96.8±7.5 in the RBC pellet.

Mean values with standard deviations were calculated for direct and indirect V_v data from both dose groups and compared to literature values (**Table 1**). Using the direct method, no differences in V_v for brain and muscle were observed when comparing naïve and B20-4.1-administered mice. Differences, expressed as $[(V_{v,B20\text{-}4.1}-V_{v,naïve})/V_{v,\ naïve}]\times100\%$, were noted in spleen (5% increase), liver (11% decrease), kidney (27% decrease), intestine (22% decrease), heart (9% decrease), lung (11% decrease), and fat (7% increase). None of these differences were statistically significant by unpaired t-test ($p>0.05$). Using the indirect method, no differences in V_v were observed between naïve and B20-4.1-administered mice for brain, muscle, and fat. Percent differences for remaining tissues, expressed as $[(V_{v,B20\text{-}4.1}-V_{v,naïve})/V_{v,\ naïve}]\times100\%$, were as follows: spleen (9% increase), liver (1% decrease), kidney (7% decrease), intestine (30% increase), heart (27% increase), and lung (21% decrease). None of these differences was statistically significant by unpaired t-test ($p>0.05$).

Excellent agreement between indirectly measured (in naïve mice) and literature V_v values, respectively, was observed for brain

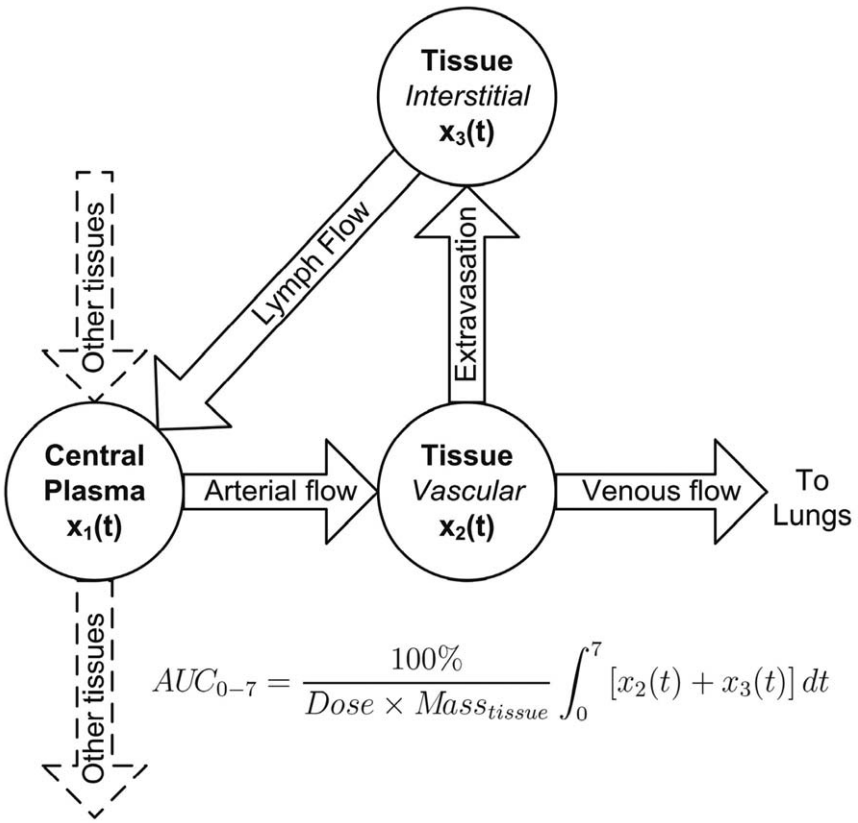

Figure 2. Diagram of physiologically-based pharmacokinetic (PBPK) model to predict antibody uptake in tissues. Shown is a typical tissue sub-model component of the PBPK model [13] used to assess the influence of parameter variability among literature and measured V_v, V_i and Q values on tissue uptake of an IgG (expressed as AUC_{0-7}). Antibody enters tissue from the central plasma compartment via arterial blood flow where it continues to the lungs via venous blood flow or returns directly to the central plasma compartment through the lymphatic system subsequent to extravasation into interstitial space. The AUC_{0-7} values listed in **Table 4** are the sum of AUCs of absolute antibody amount vs. time in the two tissue compartments (x_2 and x_3) multiplied by 100% and divided by the product of the total injected dose and mass of tissue, yielding AUC in units of %ID/g × time. Note that the muscle sub-model includes extra compartments, included in the AUC_{0-7} calculation, that describe FcRn mediated recycling and degradation of antibody.
doi:10.1371/journal.pone.0017874.g002

(11±2 vs. 9.4 μL/g) and spleen (121±29 vs. 100 μL/g) (**Table 1**). In contrast, the direct method yielded V_v values more closely matching the corresponding literature values for intestine (22±12 vs. 29 μL/g) and muscle (15±6 vs. 18.9 μL/g).

SPECT-CT imaging

The whole-body distributions of ^{99m}Tc-labeled RBCs for the two dose groups were visually assessed by single photon emission computed tomography/X ray computed tomography (SPECT-CT) imaging. Both the sagittal planar images (left) and the three-dimensional volume rendered images (right) revealed similar blood distributions for both naïve and B20-4.1-administered mice (**Figure 4**). Slight splenic uptake was evident in the SPECT-CT volume rendered images of mice in both dose groups. It should be noted that the magnitude of bladder uptake may be affected by differences in the time between injection and the start of SPECT data acquisition (98 min for naïve, 138 min for B20-4.1-administered mouse); in contrast, the mice that were used to generate the data in **Figure 3** were promptly sacrificed at 1 h post-injection of ^{99m}Tc.

Interstitial volume

From the calculated interstitial fluid volume data in naïve and B20-4.1-administered mice, mean V_i values were obtained and compared to literature values (**Table 2**). It should be noted that because the calculation of V_i requires knowledge of V_v, its accuracy is dependent on both the RBC labeling and indium-111 diethylenetriamine-*N*,*N*,*N*′,*N*′,*N*″-pentaacetic acid (^{111}In-DTPA; i.e., ^{111}In-pentetate) infusion studies. Mean V_i values for B20-4.1-administered relative to naïve mice, expressed as $[(V_{i,B20\text{-}4.1} - V_{i,naïve}) / V_{i,\ naïve}] \times 100\%$, were as follows: brain (80% increase), spleen (8% decrease), liver (20% increase), intestine (25% increase), heart (5% increase), lungs (50% increase), muscle (32% increase), and fat (11% decrease). With the exception of brain, none of these differences is statistically significant by unpaired *t*-test ($p > 0.05$). For brain, the difference exhibits a borderline statistical significance by unpaired *t*-test ($p = 0.05$).

Agreement between measured (in naïve mice) and literature V_i values, respectively, was observed for intestine (121±62 vs. 174 μL/g), heart (158±67 vs. 143 μL/g), muscle (114±19 vs. 130 μL/g), and fat (346±259 vs. 490 μL/g) (**Table 2**). The V_i value for brain in mice (20±5 μL/g) does not agree with the literature value in mice (170–190 μL/g) [14] due to an inability of the radiometal-chelate complex to cross the blood-brain barrier (**Table 2**). Similarly, the V_i value for kidneys in naïve mice (2202±462 μL/g) is also physiologically irrelevant due to renal clearance of the extracellular probe, ^{111}In-DTPA (**Table 2**).

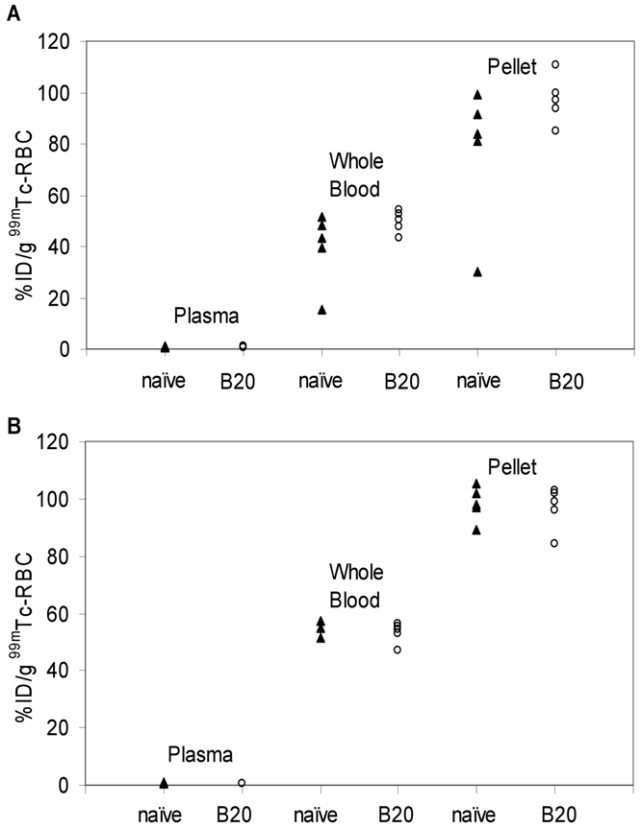

Figure 3. Measurement of technetium-99m incorporation in fractionated red blood cells. (A) Technetium-99m radioactivity, expressed as percentage of injected ^{99m}Tc dose per gram (%ID/g), in fractionated blood for mice (n = 5) whose red blood cells were labeled by the direct method. Mice were either naïve or administered a single intravenous bolus dose (10 mg/kg) of the cross-species anti-VEGF antibody, B20-4.1, 24 h prior to assay. (B) Technetium-99m radioactivity, expressed as %ID/g, in fractionated blood from mice (n = 5) whose red blood cells were labeled by the indirect method. All donor mice were naïve; recipient mice were naïve or received a single intravenous bolus dose (10 mg/kg) of the cross-species anti-VEGF antibody, B20-4.1, 24 h prior to assay.
doi:10.1371/journal.pone.0017874.g003

Organ blood flow rates

From the calculated blood flow data in naïve and B20-4.1-administered mice, mean Q values (μL/g/min) were obtained and compared to literature values (**Table 3**). Percent differences in mean Q values, expressed as $[(Q_{B20\text{-}4.1}-Q_{naïve})/Q_{naïve}]\times100\%$, were as follows: liver (27% increase), kidneys (19% increase), heart (17% increase), muscle (6% increase), fat (18% increase), spleen (9% decrease), intestine (9% decrease), and unchanged in lungs. With the exception of liver, none of these differences is statistically significant by unpaired t-test ($p>0.05$). For liver, by conventional criteria, the difference is considered to be borderline statistically significant by unpaired t-test ($p = 0.048$).

Agreement between measured (in naïve mice) and literature Q values, respectively, was observed for intestine (380±136 vs. 474 μL/g/min) and muscle (186±47 vs. 184 μL/g/min) (**Table 3**) [5]. The Q value for brain in naïve mice (12±1 μL/g/min) does not agree with the literature value (850 μL/g/min) [3,15] due to an inability of the radiometal cation, $^{86}Rb^{+}$, to cross the blood-brain barrier.

Table 1. Measured vascular volumes (V_v) in naïve and anti-VEGF-administered mice.

Tissue	V_v (Lit.)	V_v, Measured (Naïve)[h]		V_v, Measured (+ B20)	
		Direct	Indirect	Direct	Indirect
brain	9.4[a, d]	11±2	11±2	11±1	11±1
spleen	100[b, e]	149±21	121±29	156±9	133±62
liver	100[b, e]	193±34	42±8	173±24	41±8
kidney	100[b, e]	428±117	77±7	311±31	72±14
intestine	29[b, f]	22±12	8±2	17±3	10±4
heart	52.6[b, f]	45±5	30±7	41±11	38±10
lung	100[b, e]	216±46	235±111	192±75	186±26
muscle	18.9[b, f]	15±6	9±2	15±9	9±5
fat	20[c, g]	61±30	14±4	65±39	14±7

Note: Literature (Lit.) values are listed for comparison. Nude mice (n = 5) were naïve or administered a single, intravenous bolus dose (10 mg/kg) of the cross-species anti-VEGF antibody [12], B20-4.1, 24 h prior to assay. All values are reported in μL/g. Values of V_v were measured using both direct and indirect RBC labeling methods [2]. Note that the assay method can greatly influence measured V_v, especially in probe clearance organs.
[a][39].
[b][5].
[c][3].
[d]Measured using ^{3}H-inulin.
[e]For well-perfused organs 10% vascular space is assumed [5].
[f]Estimated from experimental IgG data at early time points [5].
[g]Estimated from human data.
[h]Data reproduced with permissions [2].
doi:10.1371/journal.pone.0017874.t001

PBPK simulations

Listed in **Table 4** are the simulated AUC_{0-7} values for blood and various tissues using a PBPK model parameterized with both literature and measured values of V_v, V_i, and Q, with the exception of kidney, for which literature values of V_i, were always used. The substitution of measured physiological parameter values in naïve mice resulted in changes in AUC_{0-7} values, expressed as $[(AUC_{0-7,\ measured}-AUC_{0-7,\ literature})/AUC_{0-7,\ literature}]\times100\%$, as follows: 35% increase in lungs, 15% increase in spleen, 13% increase in blood and bone, 48% decrease in liver, 46% decrease in intestine, 28% decrease in muscle, 5% decrease in kidneys, and 1% increase in heart. Note that no experimental bone measurements were made in this study. Literature values were used for this tissue in all cases, and changes in bone reflect altered plasma PK profiles.

Model-predicted AUC values may also be compared to experimentally measured values obtained from tissue distribution data (**Table 4**). The use of experimentally measured V_v, V_i, and Q values in naïve mice produced simulations that more closely matched measured AUC_{0-7} values in blood, spleen, and muscle, but not in liver, kidneys, and lungs when compared to simulations based on literature values. Specifically, the use of literature and measured parameter values, respectively, gave differences, expressed as $[(AUC_{0-7,\ model\text{-}predicted}-AUC_{0-7,\ experimental})/AUC_{0-7,\ experimental}]\times100\%$, as follows: 44% higher vs. 4% higher in muscle, 11% higher vs. 50% higher in lungs, 45% lower vs. 37% lower in spleen, 32% lower vs. 24% lower in blood, 28% lower vs. 28% lower in heart, 13% lower vs. 55% lower in liver, and 14% lower vs. 18% lower in kidneys.

Model-predicted AUC values obtained using experimentally measured values in naïve and anti-VEGF-administered mice were very similar in blood and most tissues (**Table 4**). The use of measured parameter values in naïve and B20-4.1-administered

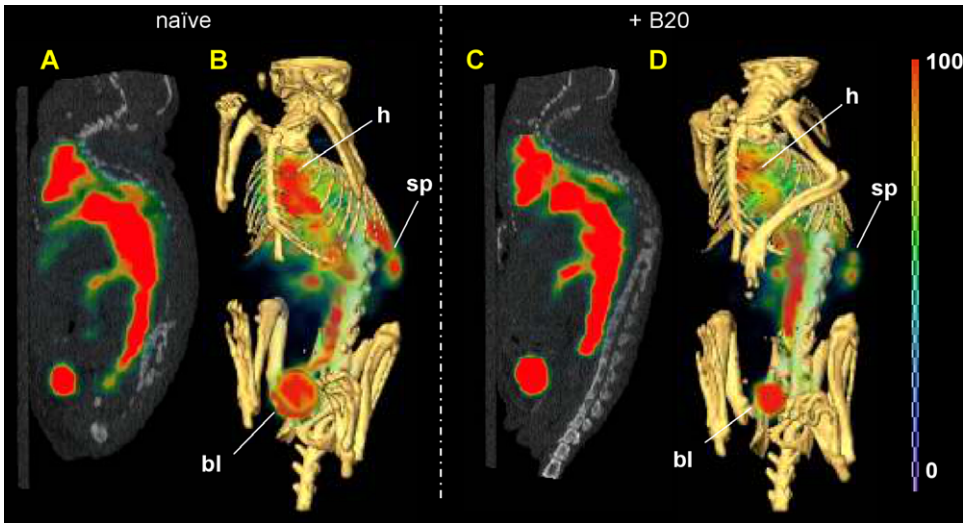

Figure 4. Noninvasive SPECT-CT imaging of blood pool in naïve and anti-VEGF-administered mice. Representative SPECT-CT blood pool images (n = 1) obtained at 98–138 min post injection in mice that were either naïve (A–B) or administered (C–D) a single intravenous bolus dose (10 mg/kg) of the cross-species anti-VEGF antibody, B20-4.1, approximately 24 h prior to image acquisition. Red blood cell labeling was performed by the indirect method. The false-colored SPECT images in arbitrary uptake units are fused onto the X-ray CT images. Both a sagittal planar image along the spine (A, C) and a corresponding three-dimensional volume rendered image (B, D) are shown for each reconstructed SPECT-CT fusion dataset. Mostly blood pool and bladder uptake are evident in the sagittal slices, while the spleen can also be clearly delineated in the right-hand side of the 3D images, just below the ribcage. The locations of visible uptake in heart (h), spleen (sp), and bladder (bl) are indicated in the volume rendering images.
doi:10.1371/journal.pone.0017874.g004

Table 2. Measured interstitial volumes (V_i) in naïve and anti-VEGF-administered mice.

Tissue	V_i (Literature)	V_i, Measured (Naïve)	V_i, Measured (+ B20)
brain	170–190[a, d]	20±5[e]	36±15[e]
spleen	200[b]	25±10	23±32
liver	200[b, g]	90±15	108±23
kidney	339[b, g]	2202±462[f]	2588±506[f]
intestine	174[b, h]	121±62	151±96
heart	143[b, h]	158±67	166±41
lung	300[b, g]	173±71	259±111
muscle	130[b, i]	114±119	150±47
fat	490[c, i]	346±259	308±121

Note: Literature values are listed for comparison. Nude mice (n = 5) were naive or administered a single, intravenous bolus dose (10 mg/kg) of the cross-species anti-VEGF antibody [12], B20-4.1, 24 h prior to assay. All values are reported in μL/g. Note that the assay method can greatly influence measured V_i values, especially in probe clearance organs.
[a][14].
[b][5].
[c][23].
[d]Tetramethylammonium (TMA^+) method; corrected for a reported 9.4 μL/g blood volume [14].
[e]Reflects inability of ^{111}In-DTPA to cross the blood-brain barrier.
[f]Non-physiologically relevant measurement due to renal clearance of ^{111}In-DTPA.
[g]Extrapolated from rat; sodium (extracellular marker) content determined in a flame photometer [22].
[h]Estimated on the basis of values for similar tissues [5].
[i]Extrapolated from rat; ^{51}Cr-EDTA method [5,23].
doi:10.1371/journal.pone.0017874.t002

Table 3. Volume velocities of regional blood flow (Q) in naïve and anti-VEGF-administered mice.

Tissue	Q, Literature	Q, Measured (Naïve)	Q, Measured (+ B20)
brain	850[a, e]	12±1[d]	12±1[d]
spleen	909[b, f]	169±105	153±71
liver	2103[b, f]	158±20*	200±35*
kidney	4881[b, g]	1172±419	1390±537
intestine	474[b, f]	380±136	346±105
heart	3828[b, f]	877±63	1026±236
lung	350[a, h]	538±150	537±262
muscle	184[b, i]	186±47	198±59
fat	190[c, j]	120±37	142±34

Note: Literature values are listed for comparison. Nude mice (n = 5) were naïve or administered a single, intravenous bolus dose (10 mg/kg) of the cross-species anti-VEGF antibody [12], B20-4.1, 24 h prior to assay. All values are reported in μL/g/min. Note that the assay method can greatly influence measured values of Q, especially in probe clearance organs.
*$p<0.05$ by unpaired t-test.
[a][3].
[b][5].
[c][40].
[d]Reflects inability of probe to cross blood-brain barrier.
[e]^{85}Sr-labeled microspheres [15].
[f]Origin of measurement not specified in literature.
[g]Extrapolated from inulin clearance rates in rat kidney [41].
[h]Bronchial flow.
[i]Measured experimentally by Rb uptake method.
[j]Rat data; method not specified [40].
doi:10.1371/journal.pone.0017874.t003

Table 4. Sensitivity of AUC_{0-7} for an antibody in mice to changes in V_v, V_i and Q.

Tissue	Model-Predicted AUC_{0-7} Values			Experimental[a]
	Lit.	Meas. (naïve)	Meas. (+ B20)	(naïve)
blood	82.5	93.0	93.1	122.2
liver	18.1	9.37	9.64	20.7
kidneys	18.7	17.8	17.1	21.8
spleen	15.4	17.7	19.4	28.1
lungs	36.7	49.5	50.2	33.1
heart	17.4	17.6	19.3	24.3
muscle	11.4	8.23	8.22	7.90
intestine	7.03	3.77	4.71	na
bone	7.58	8.55	8.56	na

Note: Comparison of model-predicted [13] and experimentally measured AUCs [%ID/g day], up to 7 days post-injection, calculated for an intact antibody in mice. All blood flow rates (Q), vascular (V_v) and interstitial (V_i) volumes were simultaneously changed from literature to measured values (see **Tables 1, 2, 3**) for these simulations, with the exception of V_i for kidneys, for which literature values were always used due to the effects of probe clearance. Measurement of V_v was accomplished using a previously reported indirect RBC labeling method [2].

[a]Data for ^{125}I-trastuzumab; reproduced with permissions [2].

doi:10.1371/journal.pone.0017874.t004

mice, respectively, gave the following differences, expressed as $[(AUC_{0-7,\ naïve} - AUC_{0-7,\ B20\text{-}4.1})/AUC_{0-7,\ naïve}] \times 100\%$: 25% higher in intestine, 10% higher in heart and spleen, 3% higher in liver, 1% higher in lungs, 0.1% higher in blood and bone, 4% lower in kidneys, and 0.1% lower in muscle.

Discussion

No significant change in three measured physiological parameters was observed for most healthy murine tissues, despite the fact that the chosen dosage of B20-4.1 was based on previously reported xenograft growth inhibition activity [16] that should result in a minimum trough concentration at steady state of ~30 μg/mL, similar to that achieved in >90% of bevacizumab patients [17]. Furthermore, selection of the 24 h time point was guided by reported statistically significant reductions in vascular density of human xenografts in mice at 24 h following anti-VEGF administration [9]. The lack of observed changes in physiology reported herein may reflect lower murine VEGF levels in healthy tissues relative to tumors in mice. Indeed, an analogous scenario has been exploited in clinical imaging of VEGF-expressing tumors with radiolabeled bevacizumab, where metastatic lesions were clearly delineated [18]. However, these findings do not preclude possible changes in additional physiological parameters such as vascular permeability to immunoglobulins; additional studies in this context are ongoing.

The blood volume measurement data indicated that the %ID/g values for whole blood were roughly half of those for the RBC pellet by either the direct or indirect labeling method, consistent with an average hematocrit value of 45% in mice [4]. Although the differences in RBC labeling efficiency between naïve and B20-4.1-administered mice were not statistically significant, the mean values in blood and RBC pellet were higher for the B20-4.1-administered mice, possibly due to anti-VEGF-mediated decrease in nitric oxide (NO) synthesis and concomitant vasoconstriction that would prolong the exposure of RBCs to Sn^{2+} and/or ^{99m}Tc pertechnetate. These observations led to the development and utilization of the indirect method to ensure that such effects were not confounding the V_v results [2].

The overall similarity in distributions of radioactivity between the two images (**Figure 4**) was consistent with the lack of significant anti-VEGF effect on measured V_v values (**Table 1**). Slight splenic uptake of ^{99m}Tc observed in SPECT-CT images was observed, as expected, due the spleen's physiological role in sequestration of RBCs [19,20,21]. Furthermore, anti-VEGF administration had no statistically significant effect on measured V_i values (**Table 2**). Because calculation of V_i requires knowledge of both vascular (^{99m}Tc-RBC) and extracellular (^{111}In-DTPA) spaces, statistical analysis of raw %ID/g ^{111}In-DTPA data was performed separately and showed no significant differences between dose groups (data not shown).

Comparing the PBPK modeling results using literature and measured parameter values demonstrates the importance of obtaining accurate values for physiological parameters. While the change in blood AUC is modest (13%) (**Table 4**), the impact of using measured physiological values is potentially high when simulating concentration-time curves within certain organs, with changes in liver and intestine AUCs of approximately 50%. Variability in AUC_{0-7} for liver is of particular significance when modeling antibody biodistribution because of its role as a clearance organ.

Although closer agreement between model predicted and experimental AUC_{0-7} values was obtained using literature V_v, V_i, and Q values in liver, kidneys, and lungs, the use of experimentally determined parameter values gave superior results in blood, muscle, and spleen (**Table 4**). Both methods demonstrated roughly comparable performance in predicting AUC_{0-7} values in heart. The excellent agreement between model predicted and experimental values in muscle is of particular significance given the inclusion of an FcRn submodel in the muscle sub-compartment of the PBPK model [13]. This nonlinear two-compartment submodel accounts for linear transfer of antibody from organ vascular space to endosomes via nonspecific bulk fluid uptake by endothelial cells, recycling of FcRn-bound antibody back into plasma, and degradation of non-FcRn-bound antibody.

Difficulty in harvesting lungs without pooling of excess blood during sacrifice may have influenced the calculated parameter values for this tissue. In addition, clearance of physiological probes may limit the validity of measurements. This effect was avoided for the vascular volume measurement by use of an indirect RBC labeling protocol to avoid contamination by non-RBC-associated ^{99m}Tc; however, ^{111}In-DTPA and ^{86}Rb are also subject to renal clearance and, in the case of ^{111}In-DTPA, possible transchelation of radiometal into metalloproteins may encourage hepatic accumulation. Due to the aforementioned complications, utilization of nominal values for lungs, liver, and kidney may be superior to the use of measured values.

The origin of values reported in the literature (**Tables 1, 2, 3**) should be carefully considered, as many are in fact assumed nominal values. For instance, a 10% vascular space is assumed for well-perfused organs (*e.g.*, kidney, lung, liver, and spleen), while, other values are estimated based on experimental uptake data of antibodies at early time points [5] (**Table 1**). In addition, multiple methods exist for measuring physiological parameters. Three distinct methods were used to obtain several V_i values that were derived from a single reference in **Table 2**: analysis of sodium content (in rat tissues) by flame photometry [22], estimation on the basis of similar tissues [5], and use of the extracellular probe, ^{51}Cr-EDTA in rat tissues [5,23]. As expected, the best agreement is found when similar methods are employed. For instance, the V_i

values for muscle and fat agree well with literature values despite the difference in species; this may be explained by similar chemical properties of the radiometal-polyaminopolycarboxylate complexes (i.e. ^{111}In-DTPA and ^{51}Cr-EDTA) used as extracellular markers. Furthermore, the impressively good agreement between the experimental (naïve) and literature Q values for muscle may be explained by the fact that the identical method of rubidium uptake was used to derive both values (**Table 3**). Interestingly, the Q value for kidney reported in the same reference [5] was extrapolated from inulin renal clearance rates, while the methods used to derive many other values could not be found in the original literature.

Of particular importance was the use of the indirect RBC labeling technique in the determination of V_v. Application of the traditional method of direct *in vivo* RBC labeling resulted in the calculation of negative interstitial volume values for many tissues, especially clearance organs (data not shown). This may be explained by interference due to non-RBC-associated ^{99m}Tc, leading to an incorrect assessment of vascular volume values. The indirect method averts such difficulties through transfusion of whole blood containing *in vivo*-purified ^{99m}Tc-labeled RBC from donor mice into study mice.

Many clinically utilized drugs, including radiopharmaceuticals for noninvasive imaging of physiological response to drug therapy [24], may also be useful as probes in invasive preclinical studies. For instance, convenient kit preparations for radiolabeling of red blood cells can allow not only clinical blood pool imaging [19,20,21,25] but also preclinical determination of vascular volume in tumors and other tissues [7,26].

Limitations exist in measuring physiological quantities, especially in regards to organs involved in renal and hepatobiliary clearance. Use of tabular physiological parameter data from a single, well-referenced source is appealing due to convenience and peer acceptance; in this context, an effort was made to select literature values (**Tables 1, 2, 3**) from heavily cited sources that are commonly used by PBPK modelers. However, for any single physiological parameter, significant variability exists among values reported by various sources; this discrepancy is often caused by differences in experimental methodology. For many modeling and simulation applications, rough estimates of physiological parameters may suffice; therefore, the use of such data is justified. Nevertheless, those who utilize such information should be aware of the experimental methods and/or estimations used to derive measured physiological parameter values so that the limitations, with respect to accuracy of PBPK model predictions, can be known.

Nominal or *in vitro* physiological parameters are often necessary in the use of PBPK models, which can lead to better understanding and predictability of drug distribution into various tissues [3,6,13,27]. PBPK models have been developed to predict *in vivo* PK solely based upon *in vitro* and *in silico* absorption, distribution, metabolism, and excretion (ADME) data together with established physiological information that describes the mammalian body [13]. Even relatively simple models can significantly improve interpretation of uptake data by allocating drug concentrations into distinct physiological compartments, such as central plasma pool and peripheral tissue. Measurable tissue physiological parameters such as fractional interstitial and blood volumes can be used in a PBPK model [13,28,29,30] to facilitate estimation of other parameters that yield additional insight into drug PK beyond what is apparent from traditional tissue distribution studies alone. For instance, correction of tissue disposition data for the fraction of drug in the vascular compartment is possible if the blood PK and tissue V_v are known; this is particularly helpful for drugs having an interstitial or cellular site of action (i.e. biophase).

In conclusion, responses to a single anti-VEGF treatment were assessed by measuring three distinct physiological parameters in nude mice. Administration of anti-VEGF had no statistically significant effect on the fractional vascular volumes of any of the tissues studied, and these findings were further supported by SPECT imaging. In addition, with the exception of a marginally significant increase in hepatic blood flow, no anti-VEGF-induced differences were detected in interstitial fluid volume and organ blood flow rates. Furthermore, PBPK model-predicted AUC_{0-7} values of an IgG were in better agreement with experimental AUC_{0-7} values in blood, spleen, and muscle when using experimentally measured compartmental volume and blood flow values when compared to simulations based on literature values. These observations may have important implications in the mechanistic understanding and prediction of antibody uptake alone or in combination with anti-VEGF therapy.

Materials and Methods

Radiopharmaceuticals

Rubidium-86 chloride (^{86}RbCl) was purchased from PerkinElmer® Life and Analytical Sciences, Inc. (Waltham, MA). Indium-111-DTPA (*i.e.* ^{111}In-pentetate) and technetium-99m (^{99m}Tc) pertechnetate were purchased from Covidien Radiopharmacy (South San Francisco, CA). All three were diluted with sterile normal saline prior to intravenous dosing. Technescan™ PYP™ (i.e. stannous pyrophosphate + ^{99m}Tc) kits for preparation of ^{99m}Tc pyrophosphate injection were purchased from Covidien Radiopharmacy (South San Francisco, CA) and used according to label instructions for the *in vivo* method of blood pool imaging with the appropriate human-to-mouse scaling.

Animal model

The protocol, housing, and anesthesia were approved (Protocol numbers 09-2490 and 09-1245) by the Institutional Animal Care and Use Committees of Genentech Laboratory Animal Resources, in compliance with the Association for Assessment and Accreditation of Laboratory Animal Care regulations. Female beige nude X-linked immunodeficient (XID) (bg.nu.xid Harlan Laboratories) mice in a 6–8-week age range were used for all measurements. Selected mice received B20-4.1, a cross-species anti-VEGF murine antibody [12], which was intravenously administered in a 10 mg/kg bolus dose 24 h prior to the V_v measurement; otherwise, consistency in handling of all mice was exercised. Selection of the B20-4.1 dose was based on previously reported xenograft growth inhibition activity at weekly doses of 10 mg/kg in immunocompromised mice [16]. In addition, a pharmacokinetic model simulation indicated that either a 5 mg/kg twice a week or 10 mg/kg weekly dosing regimen would result in a minimum trough concentration at steady state of ~30 μg/mL, similar to that achieved in >90% of bevacizumab patients [17]. Selection of the 24 h time point was guided by reported statistically significant reductions in vascular density of human xenografts in mice at 24 h following anti-VEGF administration [9].

Vascular volume

The intravascular spaces of murine tissues were measured using both direct and indirect methods as previously described [2]. The indirect method involved transfusion of radiolabeled blood from donor mice into study (i.e. recipient) mice, where donor mice had been subjected to ^{99m}Tc labeling of RBCs *in vivo* following administration of stannous (Sn^{2+}) pyrophosphate [7,25]. Use of the

clinical Technescan™ PYP™ kit is conceptually based on the original method of Sands for *in situ* (i.e. *in vivo*) RBC labeling with ^{99m}Tc [26,31]. The previous administration of stannous pyrophosphate, a component of the reconstituted Technescan kit, reduces ^{99m}Tc pertechnetate intracellularly so that it may bind to the beta chain of hemoglobin [32].

Interstitial volume

The extracellular spaces of murine tissues were measured by continuous infusion (via jugular cannulation) of the extracellular marker, ^{111}In pentetate [33,34]. A similar radiometal-polyaminopolycarboxylate complex, chromium-51- ethylenediaminetetraacetic acid (^{51}Cr-EDTA), has been previously used by others in a similar context [23]. Jugular cannulation surgeries were performed on all mice 48 h prior to measurement to allow recovery while maintaining a constant saline infusion at 20 µL/h. One group of mice received a single intravenous bolus 10 mg/kg dose of B20-4.1 24 h prior to measurement. Extracellular volume measurement was achieved by administering a constant intravenous infusion of ^{111}In pentetate (3700 kBq/mL) at a rate of 300 µL/h for exactly 1 h. Plasma and tissue samples were collected by retroorbital bleed and terminal organ harvest, respectively, and counted for radioactivity using a 1480 WIZARD™ Gamma Counter (Wallac, Turku, Finland) in the energy window for the 245-keV photon peak of ^{111}In ($t_{1/2}$ = 2.8 d) and with automatic background and decay correction. The interstitial volume (V_i) was calculated as [(*cpm* $_{TOTAL}$ of ^{111}In in 1 g tissue) − (*cpm* of ^{111}In in 1 µL of blood) × (V_v)]/(*cpm* of ^{111}In in 1 µL of plasma).

Volume velocity of organ blood flow

Regional blood flow rates (Q) in various organs and tissues were determined by sacrificing mice exactly 1 min following IV (caudal) bolus injection of a 185-kBq quantity of ^{86}RbCl [7,31,35,36,-37,38]. Tissue samples were promptly collected by terminal organ harvest and counted for radioactivity using a 1480 WIZARD™ Gamma Counter in the energy window for the 1077-keV photon peak of ^{86}Rb ($t_{1/2}$ = 18.7 d) and with automatic background and decay correction. Blood flow (Q) was calculated as (*cpm* of ^{86}Rb in 1 g tissue × CO_{total})/(*cpm* of ^{86}Rb in the total injected dose), where total cardiac output (CO_{total}) = 8000 µL/min for a mouse [4].

SPECT-CT imaging

SPECT-CT imaging of mice with ^{99m}Tc-labeled RBCs was performed as an adjunct to the *ex vivo* biodistribution studies as previously described [2]. All mice received a bolus intravenous dose consisting of ^{99m}Tc pertechnetate in 100 µL of saline for the direct method, or a 200 µL aliquot of ^{99m}Tc-labeled whole blood via the indirect method, with total injected radioactivity in the range of 10.3-14.4 MBq. Initiation of noninvasive SPECT-CT imaging was executed 98–138 min from the time of tracer injection. Image acquisition times for CT and SPECT were an average of 3 min and 12 min, respectively, with approximately 20,000 counts per projection (20 s per projection) for the latter. Calculated V_v for all tissues in the imaged mice (data not shown) agreed well with the data in **Table 1**. The SPECT and CT data was transferred to a 256×256 matrix and fused using AMIRA® graphics software (TGS, San Diego), yielding simultaneous scintigraphic and anatomic information in all tomographic scans in the 3 different spatial axes.

PBPK simulations

In order to assess the potential impact of parameter variability on physiologically-based modeling results, organ level antibody biodistribution, subsequent to a bolus dose, was simulated using a previously published PBPK model [13] (**Figure 2**). The area under the first seven days of the concentration-time curve (AUC_{0-7}) for plasma and selected tissues was calculated using parameter values taken from the literature as well as with the experimentally measured values (**Tables 1, 2, 3**) discussed herein. Note that the literature V_v and V_i values in **Tables 1, 2** were derived from reported fractional blood volumes (γ, where $\gamma = V_v/V_{tissue}$) and fractional interstitial fluid volumes (ϕ, where $\phi = V_i/V_{tissue}$) by assuming a tissue density of 1 g/mL, consistent with assumptions made in the reference from which they were obtained [5]. Comparisons of AUC_{0-7} values were made by substituting literature values of V_v, V_i and Q for liver, kidneys, intestine, spleen and lungs with experimentally measured (AUC_{0-7}) values [2]. One exception was made in that the literature value of V_i for kidney was used in all cases due to renal clearance of ^{111}In-DTPA.

Acknowledgments

The authors would like to thank Kirsten Messick, Shannon Stainton, Jose Imperio, Nicole Valle, Cynthia Young, Nina Ljumanovic, Bernadette Johnstone, Sheila Ulufatu, and Jason Ho for excellent animal studies support. Apologies are extended to those whose important and relevant work was omitted due to lack of space.

Author Contributions

Conceived and designed the experiments: CAB MGS F-PT PJF LAK. Performed the experiments: CAB GZF EEM DB MGS. Analyzed the data: CAB GZF EEM DB MGS F-PT PJF LAK. Contributed reagents/materials/analysis tools: CAB GZF EEM DB MGS. Wrote the paper: CAB GZF EEM DB MGS F-PT PJF LAK.

References

1. Boswell CA, Deng R, Lin K, Putnam WS, Lei C, et al. (2009) *In vitro-in vivo* correlations of pharmacokinetics, pharmacodynamics and metabolism for antibody therapeutics. In: Mrsny RJ, Daugherty A, eds. Proteins and Peptides: Pharmacokinetic, Pharmacodynamic, and Metabolic Outcomes. New York, NY: Informa HealthCare.
2. Boswell CA, Ferl GZ, Mundo EE, Schweiger MG, Marik J, et al. (2010) Development and Evaluation of a Novel Method for Preclinical Measurement of Tissue Vascular Volume. Mol Pharm 7: 1848–1857.
3. Brown RP, Delp MD, Lindstedt SL, Rhomberg LR, Beliles RP (1997) Physiological parameter values for physiologically based pharmacokinetic models. Toxicol Ind Health 13: 407–484.
4. Davies B, Morris T (1993) Physiological parameters in laboratory animals and humans. Pharm Res 10: 1093–1095.
5. Baxter LT, Zhu H, Mackensen DG, Jain RK (1994) Physiologically based pharmacokinetic model for specific and nonspecific monoclonal antibodies and fragments in normal tissues and human tumor xenografts in nude mice. Cancer Res 54: 1517–1528.
6. Baxter LT, Zhu H, Mackensen DG, Butler WF, Jain RK (1995) Biodistribution of monoclonal antibodies: scale-up from mouse to human using a physiologically based pharmacokinetic model. Cancer Res 55: 4611–4622.
7. Blumenthal RD, Osorio L, Ochakovskaya R, Ying Z, Goldenberg DM (2000) Regulation of tumour drug delivery by blood flow chronobiology. Eur J Cancer 36: 1876–1884.
8. Boswell CA, Lei XC, Schweiger M, Reich M, Ferl GZ, et al. (2009) *In vivo* antibody uptake and physiological measurements in mouse lung and muscle: A compartmental physiologically-based pharmacokinetic (PBPK) modeling approach. Journal of Labelled Compounds & Radiopharmaceuticals 52: S102–S102.
9. O'Connor JP, Carano RA, Clamp AR, Ross J, Ho CC, et al. (2009) Quantifying antivascular effects of monoclonal antibodies to vascular endothelial growth factor: insights from imaging. Clin Cancer Res 15: 6674–6682.
10. Kamba T, Tam BY, Hashizume H, Haskell A, Sennino B, et al. (2006) VEGF-dependent plasticity of fenestrated capillaries in the normal adult microvasculature. Am J Physiol Heart Circ Physiol 290: H560–576.

11. Ferrara N, Hillan KJ, Gerber HP, Novotny W (2004) Discovery and development of bevacizumab, an anti-VEGF antibody for treating cancer. Nat Rev Drug Discov 3: 391–400.
12. Liang WC, Wu X, Peale FV, Lee CV, Meng YG, et al. (2006) Cross-species vascular endothelial growth factor (VEGF)-blocking antibodies completely inhibit the growth of human tumor xenografts and measure the contribution of stromal VEGF. J Biol Chem 281: 951–961.
13. Ferl GZ, Wu AM, DiStefano JJ, 3rd (2005) A predictive model of therapeutic monoclonal antibody dynamics and regulation by the neonatal Fc receptor (FcRn). Ann Biomed Eng 33: 1640–1652.
14. Yao X, Hrabetova S, Nicholson C, Manley GT (2008) Aquaporin-4-deficient mice have increased extracellular space without tortuosity change. J Neurosci 28: 5460–5464.
15. Wang P, Ba ZF, Burkhardt J, Chaudry IH (1993) Trauma-hemorrhage and resuscitation in the mouse: effects on cardiac output and organ blood flow. Am J Physiol 264: H1166–1173.
16. Bostrom J, Yu SF, Kan D, Appleton BA, Lee CV, et al. (2009) Variants of the antibody herceptin that interact with HER2 and VEGF at the antigen binding site. Science 323: 1610–1614.
17. Bagri A, Berry L, Gunter B, Singh M, Kasman I, et al. Effects of anti-VEGF treatment duration on tumor growth, tumor regrowth, and treatment efficacy. Clin Cancer Res 16: 3887–3900.
18. Scheer MG, Stollman TH, Boerman OC, Verrijp K, Sweep FC, et al. (2008) Imaging liver metastases of colorectal cancer patients with radiolabelled bevacizumab: Lack of correlation with VEGF-A expression. Eur J Cancer 44: 1835–1840.
19. Atkins HL, Goldman AG, Fairchild RG, Oster ZH, Som P, et al. (1980) Splenic sequestration of ^{99m}Tc labeled, heat treated red blood cells. Radiology 136: 501–503.
20. Smith TD, Richards P (1976) A simple kit for the preparation of ^{99m}Tc-labeled red blood cells. J Nucl Med 17: 126–132.
21. Srivastava SC, Chervu LR (1984) Radionuclide-labeled red blood cells: current status and future prospects. Semin Nucl Med 14: 68–82.
22. O'Connor SW, Bale WF (1984) Accessibility of circulating immunoglobulin G to the extravascular compartment of solid rat tumors. Cancer Res 44: 3719–3723.
23. Levitt DG (2003) The pharmacokinetics of the interstitial space in humans. BMC Clin Pharmacol 3: 3.
24. Boswell CA, Bumbaca D, Pastuskovas CV, Mundo EE, Shen BQ, et al. (in press) Molecular imaging in cancer drug development. In: Chen X, ed. Molecular imaging probes for cancer research. Hackensack, NJ: World Scientific.
25. Pavel DG, Zimmer M, Patterson VN (1977) *In vivo* labeling of red blood cells with ^{99m}Tc: a new approach to blood pool visualization. J Nucl Med 18: 305–308.
26. Sands H, Shah SA, Gallagher BM (1985) Vascular volume and permeability of human and murine tumors grown in athymic mice. Cancer Lett 27: 15–21.
27. Nestorov I (2007) Whole-body physiologically based pharmacokinetic models. Expert Opin Drug Metab Toxicol 3: 235–249.
28. Garg A, Balthasar JP (2007) Physiologically-based pharmacokinetic (PBPK) model to predict IgG tissue kinetics in wild-type and FcRn-knockout mice. J Pharmacokinet Pharmacodyn 34: 687–709.
29. Green AJ, Johnson CJ, Adamson KL, Begent RH (2001) Mathematical model of antibody targeting: important parameters defined using clinical data. Phys Med Biol 46: 1679–1693.
30. Davda JP, Jain M, Batra SK, Gwilt PR, Robinson DH (2008) A physiologically based pharmacokinetic (PBPK) model to characterize and predict the disposition of monoclonal antibody CC49 and its single chain Fv constructs. Int Immunopharmacol 8: 401–413.
31. Sands H, Jones PL, Shah SA, Palme D, Vessella RL, et al. (1988) Correlation of vascular permeability and blood flow with monoclonal antibody uptake by human Clouser and renal cell xenografts. Cancer Res 48: 188–193.
32. Rehani MM, Sharma SK (1980) Site of Tc-99m binding to the red blood cell: concise communication. J Nucl Med 21: 676–678.
33. Shockley TR, Lin K, Sung C, Nagy JA, Tompkins RG, et al. (1992) A quantitative analysis of tumor specific monoclonal antibody uptake by human melanoma xenografts: effects of antibody immunological properties and tumor antigen expression levels. Cancer Res 52: 357–366.
34. Sung C, Youle RJ, Dedrick RL (1990) Pharmacokinetic analysis of immunotoxin uptake in solid tumors: role of plasma kinetics, capillary permeability, and binding. Cancer Res 50: 7382–7392.
35. Zanelli GD, Fowler JF (1974) The measurement of blood perfusion in experimental tumors by uptake of ^{86}Rb. Cancer Res 34: 1451–1456.
36. Gullino PM, Grantham FH (1962) Studies on the exchange of fluids between host and tumor. III. Regulation of blood flow in hepatomas and other rat tumors. J Natl Cancer Inst 28: 211–229.
37. Cherry SR, Carnochan P, Babich JW, Serafini F, Rowell NP, et al. (1990) Quantitative *in vivo* measurements of tumor perfusion using rubidium-81 and positron emission tomography. J Nucl Med 31: 1307–1315.
38. Hammersley PA, McCready VR, Babich JW, Coghlan G (1987) ^{99m}Tc-HMPAO as a tumour blood flow agent. Eur J Nucl Med 13: 90–94.
39. Park S, Sinko PJ (2005) P-glycoprotein and multidrug resistance-associated proteins limit the brain uptake of saquinavir in mice. J Pharmacol Exp Ther 312: 1249–1256.
40. Bjorkman S, Wada DR, Stanski DR, Ebling WF (1994) Comparative physiological pharmacokinetics of fentanyl and alfentanil in rats and humans based on parametric single-tissue models. J Pharmacokinet Biopharm 22: 381–410.
41. Bischoff KB, Dedrick RL, Zaharko DS (1970) Preliminary model for methotrexate pharmacokinetics. J Pharm Sci 59: 149–154.